Assessment of a Satellite-Based Atmospheric Budget Analysis Method Using CINDY2011/DYNAMO/AMIE and TOGA COARE Sounding Array Data

Hirohiko MASUNAGA

Hydrospheric Atmospheric Research Center, Nagoya University, Nagoya, Japan

Abstract

A satellite-based method of moisture and thermal budget analysis is examined in comparison with sounding array observations from Cooperative Indian Ocean experiment on Intraseasonal variability in the Year of 2011 (CINDY2011)/Dynamics of the Madden-Julian Oscillation (MJO) (DYNAMO)/Atmospheric Radiation Measurements (ARM) MJO Investigation Experiment (AMIE) and from the Tropical Ocean Global Atmosphere Coupled Ocean Atmosphere Response Experiment (TOGA COARE). Overall, the satellite analysis is found to quantitatively reproduce the statistical behaviors of large-scale mean vertical motion, moisture convergence, and moist static energy (MSE) convergence as observed from the sounding arrays. However, individual convective events generally do not delineate a systematic evolutionary track but are heavily spread around the ensemble mean of moisture and MSE convergences in composite space.

Next, the convective events are broken down into "developing", "off-centered", and "passing-by" classes using geostationary infrared measurements in an attempt to sort irrelevant samples that are not representative of convective dynamics. All the three composite classes show qualitatively similar evolutions except for the amplitude of variability, with genuine developing events being greatest in amplitude and passing-by disturbances being weakest. The spread among individual events is substantially reduced when the convective events immune to strong synoptic-scale influences are isolated and the contribution of horizontal advection is excluded from MSE convergence.

Keywords convection; satellite remote sensing; tropical dynamics

1. Introduction

A moisture and thermal budget analysis of the tropical atmosphere is often applied to the diagnosis of large-scale dynamics involving moist convection. Since early studies (e.g., Yanai 1961; Reed and Recker 1971; Yanai et al. 1973), in-situ observations from sounding arrays have provided excellent opportunities, while satellites had limited capabilities to profile the entire vertical structure of the atmosphere.

A breakthrough was brought about by new satellite instruments launched into the orbit in the past two decades. The Atmospheric Infrared Sounder (AIRS) and Advanced Microwave Sounding Unit (AMSU) suite (hereafter AIRS/AMSU) aboard the Aqua satellite has made it possible to observe vertical temperature profiles at a 1-km resolution (Aumann et al. 2003), and the Tropical Rainfall Measuring Mission (TRMM) and CloudSat radars have enabled us to study the internal structure of clouds and precipitation to a great detail.

Taking advantage of such recent technological advances in remote sensing from space, Masunaga (2013) devised a budget analysis scheme that is designed for an exclusive use of satellite data. Masunaga and L'Ecuyer (2014) further advanced this meth-

Corresponding author and present afffilation: Hirohiko Masunaga, Institute for Space-Earth Environmental Research, Nagoya University, Furo-cho Chikusa-ku, Nagoya 464-8601, Japan
E-mail: masunaga@hyarc.nagoya-u.ac.jp

odology to derive large-scale mean vertical velocity. The aim of this study is to shed new light on the long-standing problems in tropical meteorology regarding the interplay of convective clouds and large-scale dynamics from the thermodynamic budget perspectives. Numerous studies have been conducted with focus on gross moist stability (GMS) (Neelin and Held 1987; Raymond et al. 2009). The analysis method of Masunaga and L'Ecuyer (2014) provides an observational tool to diagnose tropical dynamics in light of GMS in a way, unlike reanalysis datasets, fully independent of parameterized physics.

The strategy of Masunaga (2013) is unique in a few aspects compared with conventional approaches employed for thermodynamic budget analysis. First, it is applied to a large number of satellite snapshots projected onto a composite time axis defined with respect to the timing of convective occurrence (Masunaga 2012a). This statistical approach circumvents the practical limitation that individual meteorological events are unable to monitor continuously over time from low Earth orbiting (LEO) satellites. Second, a new strategy has been explored to compute large-scale mean horizontal convergence (and hence vertical motion) without direct knowledge of wind estimates since no present spaceborne sensor measures the vertical structure of winds (see Section 2 for a summary of technical details). This non-traditional method has yet to be validated against independent sources of observations.

In this study, sounding array data from two field campaigns are utilized as the reference for an assessment of the satellite analysis. The primary reference dataset analyzed here was acquired during the three field campaigns conducted closely in collaboration as follows: Cooperative Indian Ocean experiment on Intraseasonal variability in the Year of 2011 (CINDY2011), Dynamics of the Madden-Julian Oscillation (MJO) (DYNAMO), and Atmospheric Radiation Measurements (ARM) MJO Investigation Experiment (AMIE) (Yoneyama et al. 2013). A secondary reference is the data from the Tropical Ocean Global Atmosphere Coupled Ocean Atmosphere Response Experiment (TOGA COARE) (Webster and Lukas 1992). It is not attempted to restrict satellite snapshots to the regions and periods of the field campaigns, because the satellite-based composite time series by design require a far greater volume of samples to be statistically robust. Therefore, the comparison will not be precise on an event-by-event basis but relies on the assumption that the fundamental characteristics of tropical convection and its thermodynamic environment are nonetheless shared among all the measurements analyzed (see Section 5 for discussion on this issue).

The data and composite analysis method are first described in Section 2, and the results from the composite analysis are presented in Section 3. The composite analysis is examined with a morphological diagnosis based on geostationary satellite imagery in Section 4 and discussed further in Section 5. The present findings are summarized in Section 6.

2. Data and method

The datasets and analysis method are outlined in this section.

2.1 LEO satellite observations

The vertical profiles of humidity and temperature observed from the AIRS/AMSU serve as a primary input into the moisture and thermal budget analysis. The budget equation is completed with additional parameters such as precipitation and surface wind retrieved from other A-Train instruments and Quick Scatterometer (QuikSCAT). The Tropical Rainfall Measuring Mission (TRMM) Precipitation Radar (PR) is employed to determine the timing of precipitation occurrence. The target area is global tropical oceans between 15°S and 15°N and the analysis period spans from December 1, 2002 to November 30, 2009.

The overall analysis procedure is briefly outlined below. Satellite soundings collected over the entire analysis period are sorted by the observational time differences relative to the moment when the TRMM detects precipitation. The accumulated snapshots of temperature and moisture are averaged into a composite time series as a statistical representation of the atmospheric variability over time associated with the development of moist convection (Masunaga 2012a). The composite time series is constructed from ~ 30,000 satellite snapshots within an hourly bin at the time of peak convection and more than ~ 300,000 for hours away from active convection. The sample size varies over time because infrared soundings become more difficult to sample as cloud cover increases.

The composite moisture and dry static energy (DSE) are vertically integrated over the free troposphere (FT), defined here as the entire tropospheric layer above cloud base (CB), and the sub-cloud layer (SC) so that the FT convergence of moisture, q, and DSE, s, is deduced as a residual term in the budget equations:

$$-\langle\nabla\cdot q\mathbf{v}\rangle_{\mathrm{FT}} = \frac{\partial}{\partial t}\langle q\rangle + \langle\nabla\cdot q\mathbf{v}\rangle_{\mathrm{SC}} - \bar{E} + \bar{P}, \qquad (1)$$

and

$$-\langle\nabla\cdot s\mathbf{v}\rangle_{\mathrm{FT}} = \frac{\partial}{\partial t}\langle s\rangle + \langle\nabla\cdot s\mathbf{v}\rangle_{\mathrm{SC}} - \bar{S} - L\bar{P} - \langle Q_R\rangle, \qquad (2)$$

where $\langle\cdots\rangle_{\mathrm{FT}}$ and $\langle\cdots\rangle_{\mathrm{SC}}$ designate the vertical integral over FT and SC, respectively, and the notation follows the convention for meteorological parameters. The overbar indicates horizontal averaging over a circular large-scale domain. The large-scale domain diameter is chosen in this study to be 600 km unless otherwise noted so it is roughly comparable in size to the CINDY2011/DYNAMO/AMIE (hereafter CINDY/DYNAMO for brevity) and TOGA COARE sounding arrays.

Under the assumption that SC convergence is determined with QuikSCAT wind, the RHS of equations (1) and (2) can be evaluated solely by satellite measurements currently available (Masunaga 2013). The evolution of moisture and DSE convergences on the LHS thus may be derived as constrained by the set of satellite observations projected onto the composite time axis.

The vertically integrated convergence of moisture and DSE may be interpreted mathematically as lower- and upper-troposphere weighted convergence profiles, so Eqs. (1) and (2) together could give a clue for the vertical structure of horizontal divergence and hence of vertical velocity, ω. Masunaga and L'Ecuyer (2014) extended this idea to a satellite-based scheme to estimate a full vertical profile of large-scale mean vertical motion, facilitated by a vertical mode decomposition of ω into the first baroclinic, second baroclinic, and shallow modes in addition to a time-independent, background ω profile. Two of the three equations to solve the three ω modes are as follows:

$$\sum_i \left\langle q\frac{\partial\omega_i}{\partial p}\right\rangle_{\mathrm{FT}} = -\langle\nabla\cdot q\mathbf{v}\rangle_{\mathrm{FT}} + \langle\mathbf{v}\cdot\nabla q\rangle_{\mathrm{FT}}, \qquad (3)$$

$$\sum_i \left\langle s\frac{\partial\omega_i}{\partial p}\right\rangle_{\mathrm{FT}} = -\langle\nabla\cdot s\mathbf{v}\rangle_{\mathrm{FT}} + \langle\mathbf{v}\cdot\nabla s\rangle_{\mathrm{FT}}, \qquad (4)$$

where the subscript i represents each vertical mode. The first term on the RHS of Eqs. (3) and (4) (convergence) are as given by Eqs. (1) and (2). Although relatively minor in the current applications (see Section 5), the second term or horizontal advection, can also be determined by an iterative procedure so as to satisfy the given observations. The third equation is

the boundary condition at CB imposed by QuikSCAT wind,

$$\bar{\omega}_{\mathrm{CB}} = \langle\nabla\cdot q\mathbf{v}\rangle_{\mathrm{SC}}. \qquad (5)$$

Further technical details may be found in the references mentioned above.

2.2 Sounding arrays

Two adjacent sounding arrays, or the northern sounding array (NSA) and southern sounding array (SSA), were established over the central Indian Ocean for CINDY/DYNAMO (Yoneyama et al. 2013). NSA and SSA each comprise four land or ship sites that are approximately 5° to 8° apart along each side of the array, facing each other nearly on the equator where two of the six sites are shared. Array-averaged estimates of meteorological parameters are provided from the Colorado State University (CSU) DYNAMO product version 2a (Johnson and Ciesielski 2013). The analysis period spans three months from October 1 to December 31, 2011. The TOGA COARE intensive flux array (IFA) is comparable in size and in latitude to the CINDY/DYNAMO arrays but is located in the western tropical Pacific to the east of the maritime continent. The CSU TOGA COARE IFA-averaged product version 2 is analyzed (Ciesielski et al. 2003) for four months from November 1, 1992 to February 28, 1993.

In this study, moisture and MSE convergences are calculated with vertical and horizontal advections from the CINDY/DYNAMO and TOGA COARE datasets using the identity relation as follows:

$$-\langle\nabla\cdot q\mathbf{v}\rangle = \left\langle q\frac{\partial\omega}{\partial p}\right\rangle - \langle\mathbf{v}\cdot\nabla q\rangle = -\left\langle\omega\frac{\partial q}{\partial p}\right\rangle - \langle\mathbf{v}\cdot\nabla q\rangle,$$
$$(6)$$

$$-\langle\nabla\cdot h\mathbf{v}\rangle = \left\langle h\frac{\partial\omega}{\partial p}\right\rangle - \langle\mathbf{v}\cdot\nabla h\rangle = -\left\langle\omega\frac{\partial h}{\partial p}\right\rangle - \langle\mathbf{v}\cdot\nabla h\rangle,$$
$$(7)$$

where h indicates MSE and angle brackets designate the vertical integral over the entire troposphere from 50 hPa to surface.

The time series of moisture and MSE convergences are composited with respect to precipitation occurrences so they are analyzed in a format comparable as closely as possible to the satellite-based estimates. For the CINDY/DYNAMO arrays, the base points that define time zero in composite time series are given by local maxima in the temporal sequence of surface precipitation. The 3-hourly TRMM 3B42
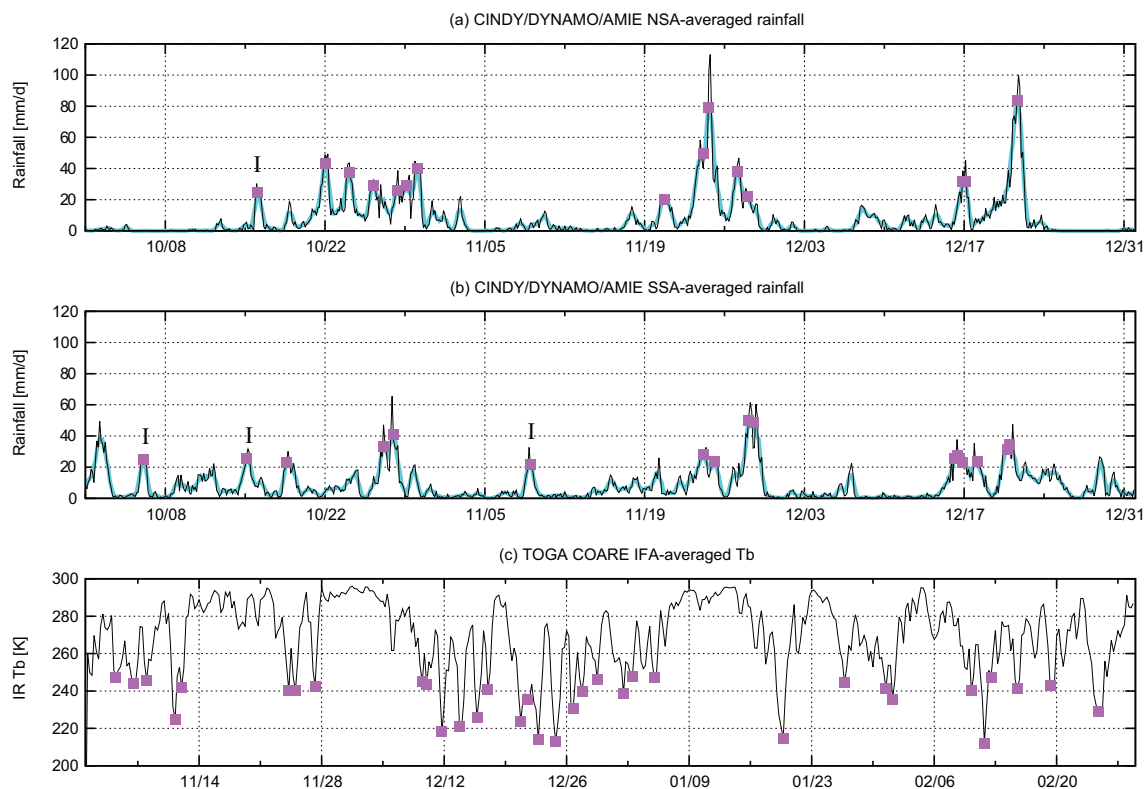
Fig. 1.   (a) Raw (black) and smoothed (cyan) time series of CINDY/DYNAMO NSA-averaged precipitation. The precipitation peaks selected for the compositing base points are marked with magenta squares. Isolated events analyzed later (see Section 5) are indicated by "I." (b) As (a) but for CINDY/DYNAMO SSA-averaged precipitation. (c) As (a) but for TOGA COARE IFA-averaged infrared brightness temperature from GMS. No smoothed time series is plotted for (c).

version 7 product (Huffman et al. 2007) averaged over each array is smoothed over time by ±6-hour running mean to filter high-frequency noises. The base points are selected at times when the peaks in the smoothed precipitation exceed one standard deviation, 11.2 mm d^{-1}, above the average, 8.54 mm d^{-1}, as obtained from the entire time sequence of the NSA and SSA precipitation. The precipitation maxima too close to either end of the period have been excluded so as to assure that a ±72-h long sequence is sampled around every base point. Figures 1a, b shows the time series of precipitation and its peaks chosen as the base points, which are 15 in total for NSA and 17 for SSA. A majority of the selected base points appear to have occurred in association with the three MJO events observed in late October, late November, and middle December (Yoneyama et al. 2013) with a few exceptions. An analogous compositing approach has been applied to in-situ polarimetric radar analysis

from CINDY/DYNAMO (Zuluaga and Houze 2013; Powell and Houze 2013).

The base points for TOGA COARE are defined similarly but using minima in Geostationary Meteorological Satellite (GMS) infrared brightness temperature (T_b) averaged over IFA because any adequate precipitation dataset is unavailable for the TOGA COARE period. The array-averaged infrared T_b is already smooth by nature and hence a running-mean filter is not applied. Totally 35 base points, determined when the infrared minima are colder than one standard deviation (20.2 K) below the mean (269 K), are identified for TOGA COARE.

3.   Composite time series

3.1   Large-scale mean vertical motion

The evolution of large-scale mean vertical motion (ω) from the satellite, CINDY/DYNAMO, and TOGA COARE composites is illustrated in Fig. 2. Each time
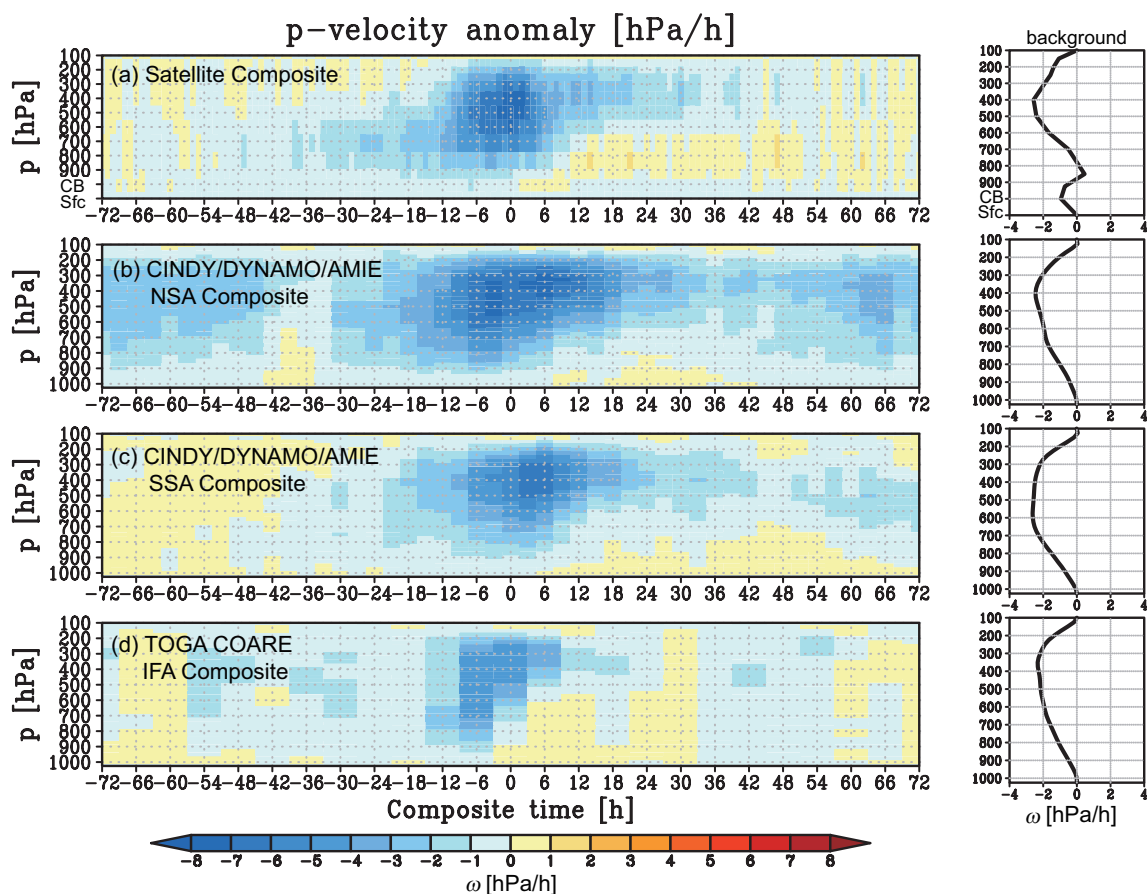
Fig. 2. (a) Satellite-based composite time series of large-scale mean vertical motion (ω) anomaly [hPa h^{-1}]. The time axis spans 72 h before and after the time of precipitation occurrence at $t = 0$. The background ω is plotted on the right. The two lowest levels correspond to surface (Sfc) and cloud base (CB), and thus vary in pressure with time. (b) As (a) but for CINDY/DYNAMO NSA-averaged ω, for which the temporal mean over the entire period defines the background. All pressure levels are fixed over time. (c) As (b) but for CINDY/DYNAMO SSA-averaged ω. (d) As (b) but for TOGA COARE IFA-averaged ω.

sequence is shown in terms of the anomaly against the background profile plotted in the right column. A rapid development of large-scale updraft throughout the troposphere several hours prior to the peak precipitation (time zero) is a consistent property shared by all the four composites. Furthermore, an upper-tropospheric layer of updraft lingering after $t = 0$ as ω diminishes more quickly in the lower troposphere is commonly observed, suggestive of a buildup of the second baroclinic (or stratiform) mode. It is noted that the sounding array data are not required by design to exhibit baroclinic mode signatures, which in contrast are built in the satellite composite algorithm. Therefore, the comparison offers a verification of the mode decomposition technique used for the satellite analysis.

One can see several features specific to certain composites. A layer of updraft confined to below 500 hPa emerges and thickens as time progresses to the full depth of the troposphere in the satellite composite (Fig. 2a), while such a gradual deepening is not evident in the sounding array measurements. The CINDY/DYNAMO NSA composite (Fig. 2b) shows a hint of periodicity with a cycle of 2 to 3 days, consistent with the striking influence of 2-day disturbances on NSA as documented by Johnson and Ciesielski (2013). The variability of ω is somewhat weaker in amplitude for TOGA COARE than the other composites (Fig. 2d), presumably because infrared minima are less efficient than precipitation maxima to sharply

define the composite temporal sequences. It may be concluded that the satellite composite reasonably captures the fundamental characteristics in the evolution of ω anomaly, given that the differences between the satellite and sounding array observations are no greater than the diversity among the three sounding arrays.

However, the satellite composite contrasts against the CINDY/DYNAMO and TOGA COARE composites in the background ω profile. Although they all agree in that a weak top-heavy structure dominates the background vertical motion, the satellite composite exhibits a shallow secondary peak below 800 hPa that is absent in the sounding array composites. The disagreement may be partly ascribed to the procedural differences in calculating the background vertical motion. The background profile is simply the temporal mean for the sounding array composites while determined so as to be as close as possible to the radiatively driven subsidence under the energy budget constraint for the satellite composite [see Masunaga and L'Ecuyer (2014) for technical details]. The present satellite-based algorithm should be carefully assessed for validity to mitigate potential methodological problems, although the secondary peak may not necessarily be fictitious because a shallow large-scale circulation is present widely over the tropical oceans as well as deep Hadley and Walker cells (Trenberth et al. 2000; Zhang et al. 2008).

3.2   Moisture convergence and MSE convergence

Next, vertically integrated moisture and MSE convergences are examined. The composite time series from CINDY/DYNAMO and TOGA COARE are compared with the satellite estimates in Fig. 3. The satellite estimate of moisture convergence (Fig. 3a) follows an evolutionary track closely resembling the sounding array measurements, where moisture convergence increases toward the peak at time zero and then turns to a decrease. The sounding arrays, in particular, CINDY/DYNAMO NSA, exhibit a somewhat larger moisture convergence than the satellite during hours away from time zero. This might originate from preceding or subsequent disturbances, e.g., two-day disturbances as we have seen in the NSA-composite vertical motion (Fig. 2b), that have not entirely been averaged. On the other hand, the discrepancy near time zero, may be partly because of a minor but non-negligible difference in the size of the analysis domain. A ±200-km perturbation to the large-scale domain diameter is indicated by gray shade as a measure of the dependence upon the

domain size, indicating a striking enhancement of sensitivity around the time of peak convection.

MSE is weakly diverging until a sharp onset of MSE divergence that occurs as the convection intensifies around time zero (Fig. 3b). The satellite and sounding array composites are in remarkable agreement throughout the evolution of MSE convergence. The timing and magnitude of variability are surprisingly consistent, given the fact that all the composites are constructed with various sets of samples acquired from different regions and periods of time and even in different analysis strategies.

It is the ensemble mean over different events that is plotted in Fig. 3 for the sounding array composites. However, the ensemble mean may not always be representative of individual convective events. Figure 4 shows moisture convergence for all individual events projected onto composite space as well as their ensemble mean. The spread over individual samples is so large that it would be difficult to clearly identify a systematic evolution without averaging over a number of samples. Individual events relatively well converge around the ensemble average for CINDY/DYNAMO SSA, while for NSA, some outliers deviate far off the mean from time to time. The TOGA COARE IFA composite is even noisier and the amplitude of moisture convergence enhancement is least prominent, as one might expect from the relatively muted variability in IFA-averaged vertical motion (Fig. 2c).

The event-by-event spread may seem much larger for MSE convergence (Fig. 5) than that for moisture convergence. However, it should be noted that the ordinate in Fig. 5 measures a much narrower range than in Fig. 4 since moisture convergence and dry static energy (DSE) convergence largely offset each other in magnitude when combined into MSE convergence. Possible origins of the spread will be discussed in Section 5.

4.   Developing and passing-by disturbances

The composite time series from satellite measurements shown above and in the previous papers (Masunaga 2012a, b, 2013, 2014; Masunaga and L'Ecuyer 2014) were constructed in the Eulerian framework, where it is unable to determine whether the detected convective system stays within the analysis domain during the entire evolution or swiftly moves in and out of the domain without completing a life cycle. In the latter case, the composite evolution may not directly result from the dynamic processes involving the buildup and dissipation of convective systems. Hence, it is unclear that the dynamic evolution of

(a) Moisture Convergence
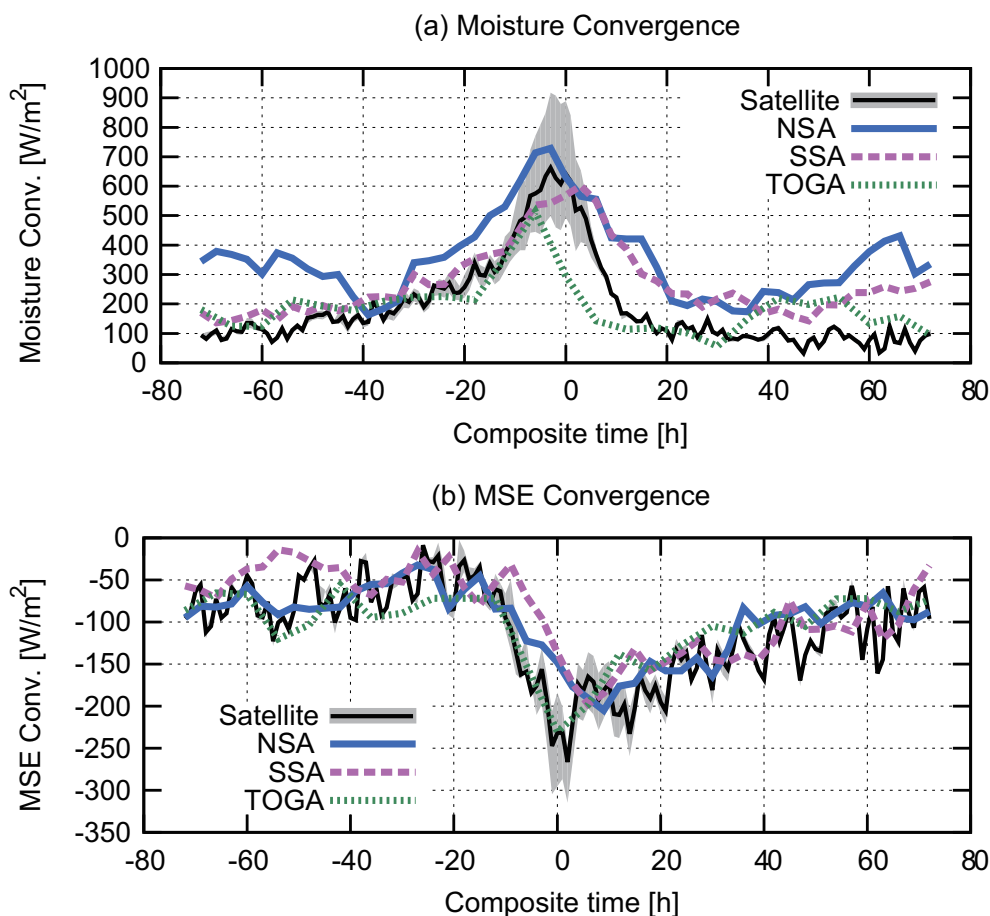
(b) MSE Convergence

Fig. 3. (a) Composite time series of vertically integrated moisture convergence [W m^{-2}] from the CINDY/ DYNAMO NSA (blue solid), CINDY/DYNAMO SSA (magenta dashed), TOGA COARE IFA (green dotted), and satellite estimates (black curve with gray shade). The width of the gray shade shows a range of large-scale domain diameters being varied from 400 km to 800 km, while the control analysis (600 km) is indicated by black line. Only the ensemble mean is plotted for the sounding array composites. (b) As (a) but for MSE convergence.

convective systems is captured to its entirety from the current compositing technique. This problem would create a serious ambiguity in the physical interpretation of the analysis results.

In this section, it is attempted to address this concern by means of a morphological diagnosis of geostationary satellite imagery over the central Indian Ocean during CINDY/DYNAMO. These observations are useful, as demonstrated below, for separately assessing the composite evolution of evolving convective systems and those without systematic evolution. On the other hand, the satellite-based composite is comprised of sporadic snapshots sampled out of context regarding whether the parent convective system is developing or non-developing. In this section,

the individual convective events captured during CINDY/DYNAMO are examined to sort how many events are dynamically evolving or merely passing through the array. Implications obtained in this manner are expected to be applicable to the satellite composite as well as the sounding array, given that the satellite-based and sounding-array composites share fundamental characteristics as shown in Figs. 2–5. As such, the strategy here is to exploit the statistics from sounding-array measurements to study the nature of representative convective systems that constitute the composite time series from satellite observations. The TOGA COARE data are not utilized for this section to reduce the analysis burden.

(a) CINDY/DYNAMO/AMIE NSA Composite

(b) CINDY/DYNAMO/AMIE SSA Composite

(c) TOGA COARE IFA Composite
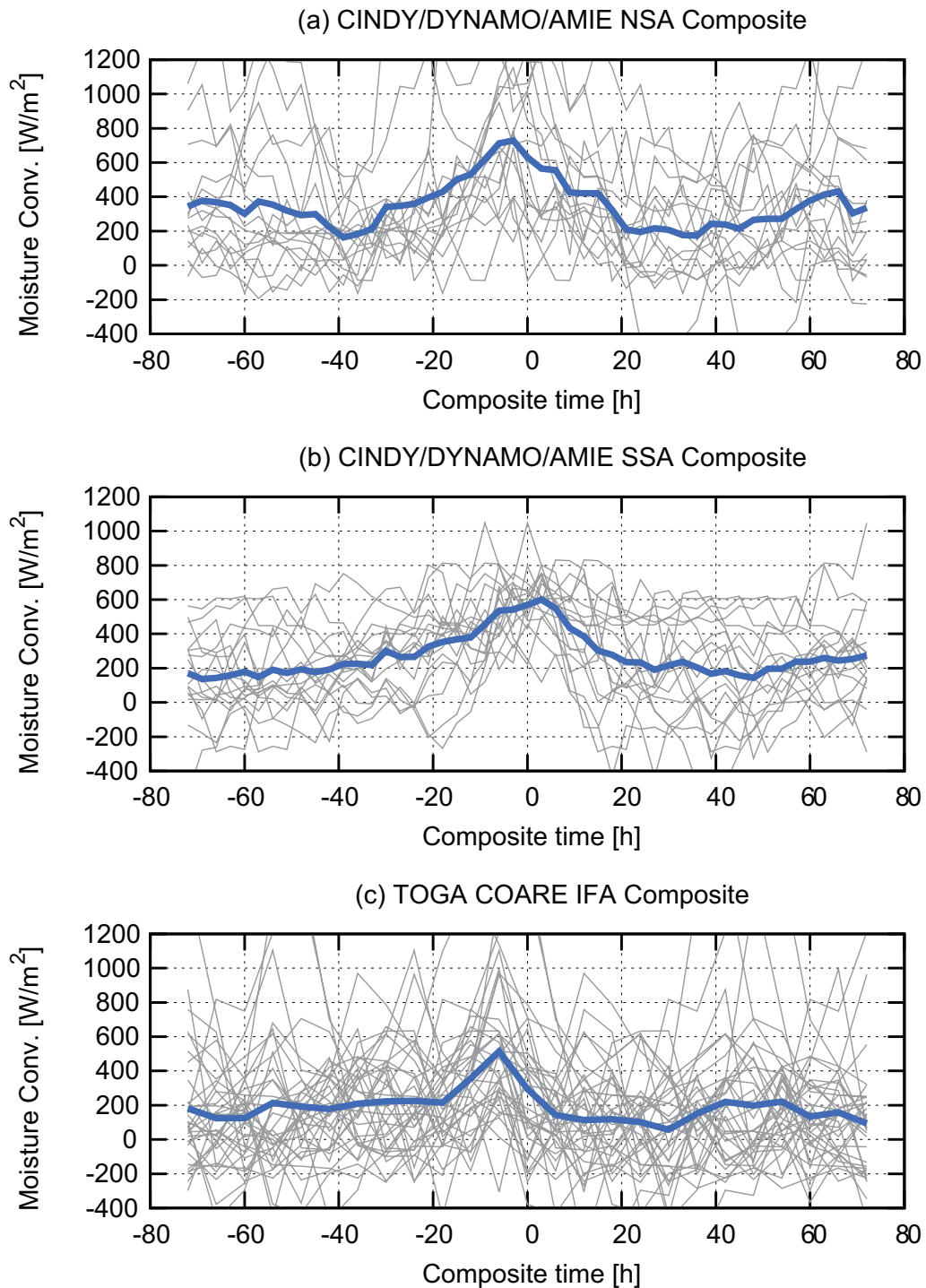
Fig. 4. (a) Vertically integrated moisture convergence [W m^{-2}] in composite space for CINDY/DYNAMO NSA. The time axis spans 72 h before and after the time of precipitation occurrence at $t = 0$. Individual samples are drawn in gray and their ensemble mean in blue. (b) As (a) but for CINDY/DYNAMO SSA. (c) As (a) but for TOGA COARE IFA.

(a) CINDY/DYNAMO/AMIE NSA Composite

(b) CINDY/DYNAMO/AMIE SSA Composite

(c) TOGA COARE IFA Composite
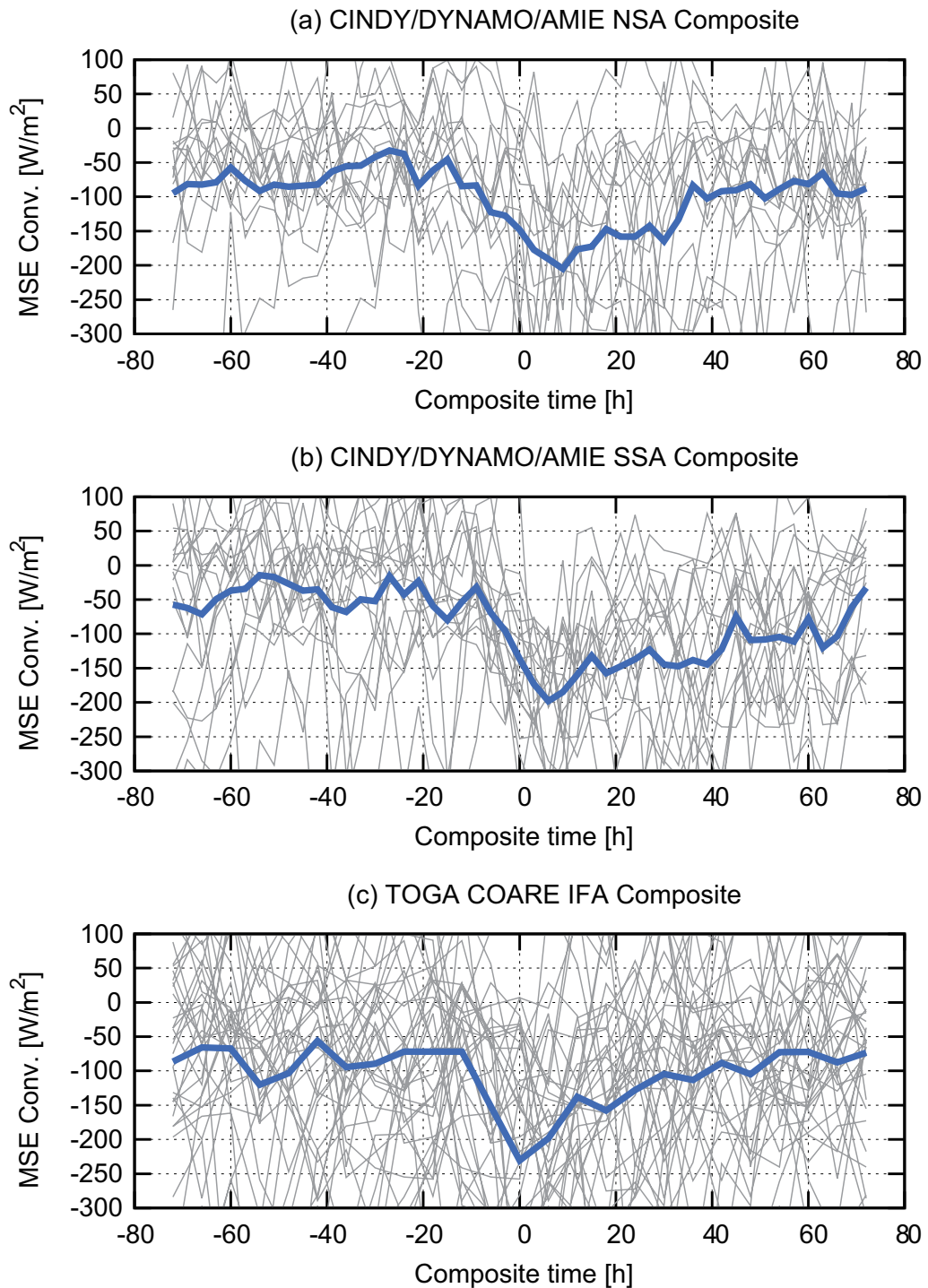
Fig. 5.   As Fig. 4 but for vertically integrated MSE convergence.

4.1   Classification of convective disturbances

Half-hourly maps from Meteosat-7 infrared T_b are analyzed for categorizing observed disturbances into three "composite classes" of developing, off-centered, and passing-by categories. The developing class comprises "bona-fide" cases where convective
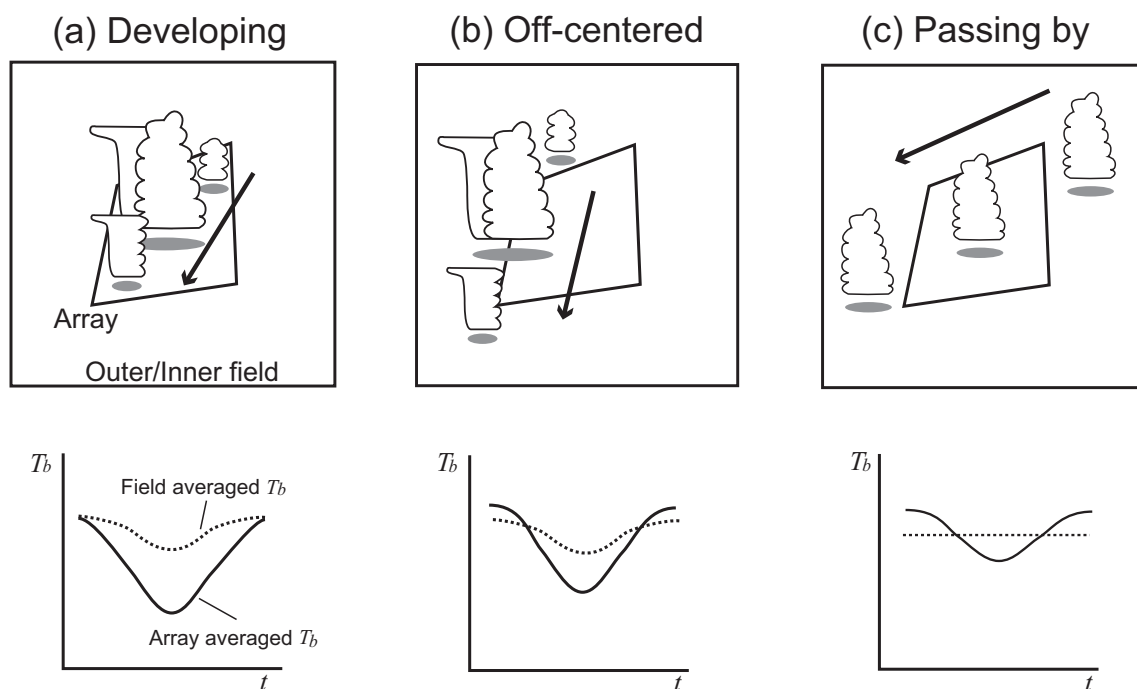
Fig. 6. Schematic to illustrate the classification method into (a) developing, (b) off-centered, and (c) passing-by classes. The top row depicts disturbances marching through the sounding array with its temporal order indicated by an arrow. The bottom graphs are the time series of infrared brightness temperature spatially averaged over the sounding array (solid) and the encompassing field (dotted).

systems largely evolve within a sounding array (NSA or SSA). In the off-centered class, the life cycle of a convective system is partially captured, whereas a main portion of the system resides outside the domain. The disturbance is classified as a passing-by system when the temporal modulation likely results from the advective effects as the disturbance enters and leaves the array, and thus may not well reflect the convective life cycle.

The classification is made on the basis of time-series segments of infrared T_b sampled around each compositing base point. Next, the infrared T_b is spatially averaged over the sounding array and over a broader field. Here the "field," or later termed more specifically as "inner/outer field," refers to a reference domain encompassing the sounding array, introduced for reasons that will become clear below. As illustrated in Fig. 6, passages of disturbances would be recorded in infrared T_b in distinguishable ways for the different composite classes. Infrared T_b would vary with time in a coherent manner between the array and field averages for developing disturbances, although cold cloud emissions are heavily smoothed in the

field average (Fig. 6a). This pattern would be slightly modified when the disturbance track is off-centered from the array, resulting in a warmer array-averaged T_b than the field average during the times when cold clouds stay outside the array (Fig. 6b). In cases where the disturbance only passes by without any appreciable development, the field averaged T_b would be practically invariant over time while the array-averaged T_b should be modulated as the disturbance moves in and out of the array (Fig. 6c). As such, an inspection of the array- and field-averaged T_bs could offer a qualitative guidance to differentiate developing, off-centered, and passing-by disturbances.

This idea is tested with Meteosat data during the CINDY/DYNAMO (Figs. 7, 8). Two field boxes with different sizes (hereafter inner and outer fields) are examined in order to ensure that the classification is not affected by the choice of field size. The inner field is a rectangular area bound at 2°S, 8°N, 70°E, and 83°E for NSA and at 9°S, 1°N, 70°E, and 83°E for SSA. The outer field is a broader region containing the inner field inside and is bound at 4°S, 10°N, 65°E, and 88°E, for NSA and at 11°S, 3°N, 64°E, and 88°E
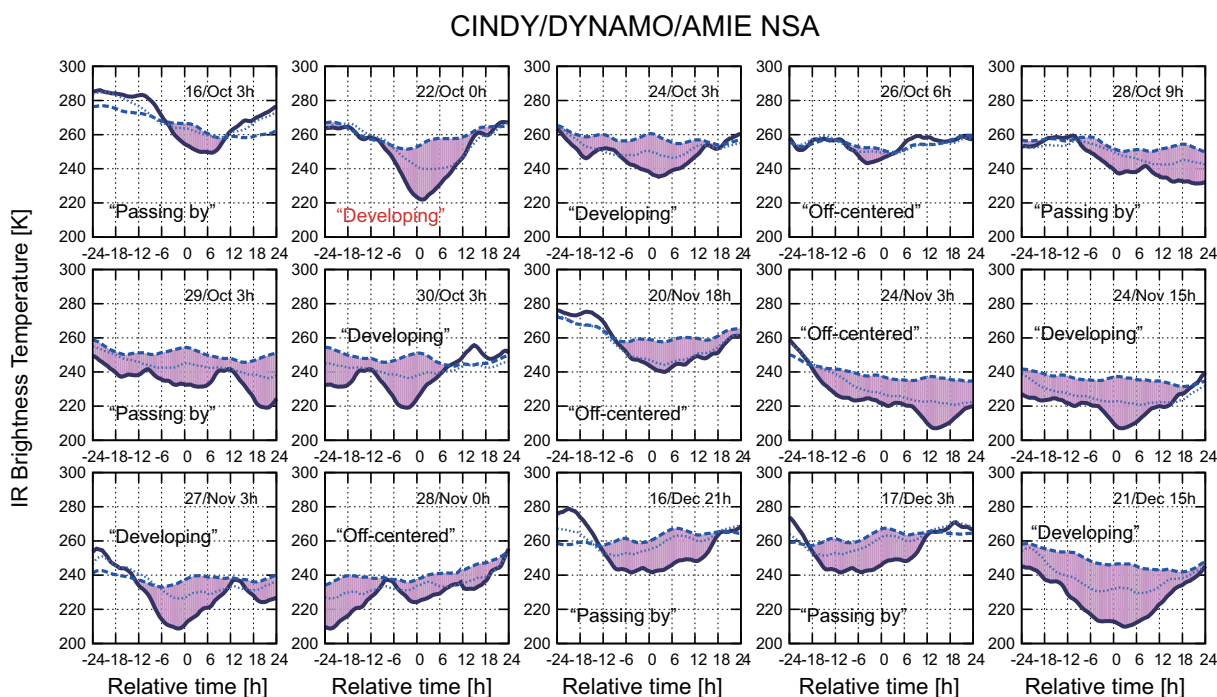
Fig. 7. Temporal sequences of Meteosat infrared T_b around every base point defined for CINDY/DYNAMO NSA. The abscissa shows hours relative to the base point as time-stamped on the top-right corner of each panel. Infrared T_b is spatially averaged over the sounding array (solid) and the inner and outer fields (dotted and dashed, respectively). The sector bound between the array averaged T_b and the outer-field averaged T_b is shaded where the latter exceeds the former for visual guidance. The composite class is identified as indicated, and is highlighted in red for the representative cases selected for Fig. 9.

for SSA. Figures 7 and 8 imply that overall the inner and outer fields appear to provide consistent references for the classification as illustrated in the schematics (Fig. 6).

However, actual observations shown by Figs. 7 and 8, are often not clearly classifiable in light of the idealized schematic illustrated in Fig. 6. The classification is subjectively made by visual inspection since it is difficult to implement an automated procedure in an objective fashion. To briefly assess the performance of the classification scheme, geographical maps of infrared T_b for selected events are presented in Fig. 9. The 22 October event observed in the NSA (second from left in the top row of Fig. 7) is selected as a typical developing case resembling the schematic of Fig. 6a. A sequence of T_b images for this event are shown in Fig. 9a. Two major disturbances are present at 12 h UTC on October 21, one to the west and another to the east of the array, but each of them break apart as time proceeds. In fact, pieces of smaller clouds inside the array gradually organize

themselves into a new disturbance toward 0 h UTC on October 22, which subsequently begins to resolve as emanating remnant high clouds away from the array. An example for the off-centered class is the November 9 event captured in the SSA (leftmost of the second row in Fig. 8). The field-averaged T_b is initially colder than the array average, suggesting that a convective disturbance stays off the array in the beginning as evidenced by Fig. 9b. An entire life cycle of the disturbance is clearly traceable from the sequential images, although the array captures only a portion of the evolution.

The October 18 SSA event (middle of the top row in Fig. 8) is chosen as a passing-by case since T_b hardly changes when averaged over the outer array. However, this particular case does not provide clear evidence for a disturbance traveling across the area as speculated by Fig. 6c as far as one can tell from Fig. 9c, where patches of clouds irregularly change in shape and size over time. It is often the case in reality, as mentioned above, that a convective disturbance

CINDY/DYNAMO/AMIE SSA
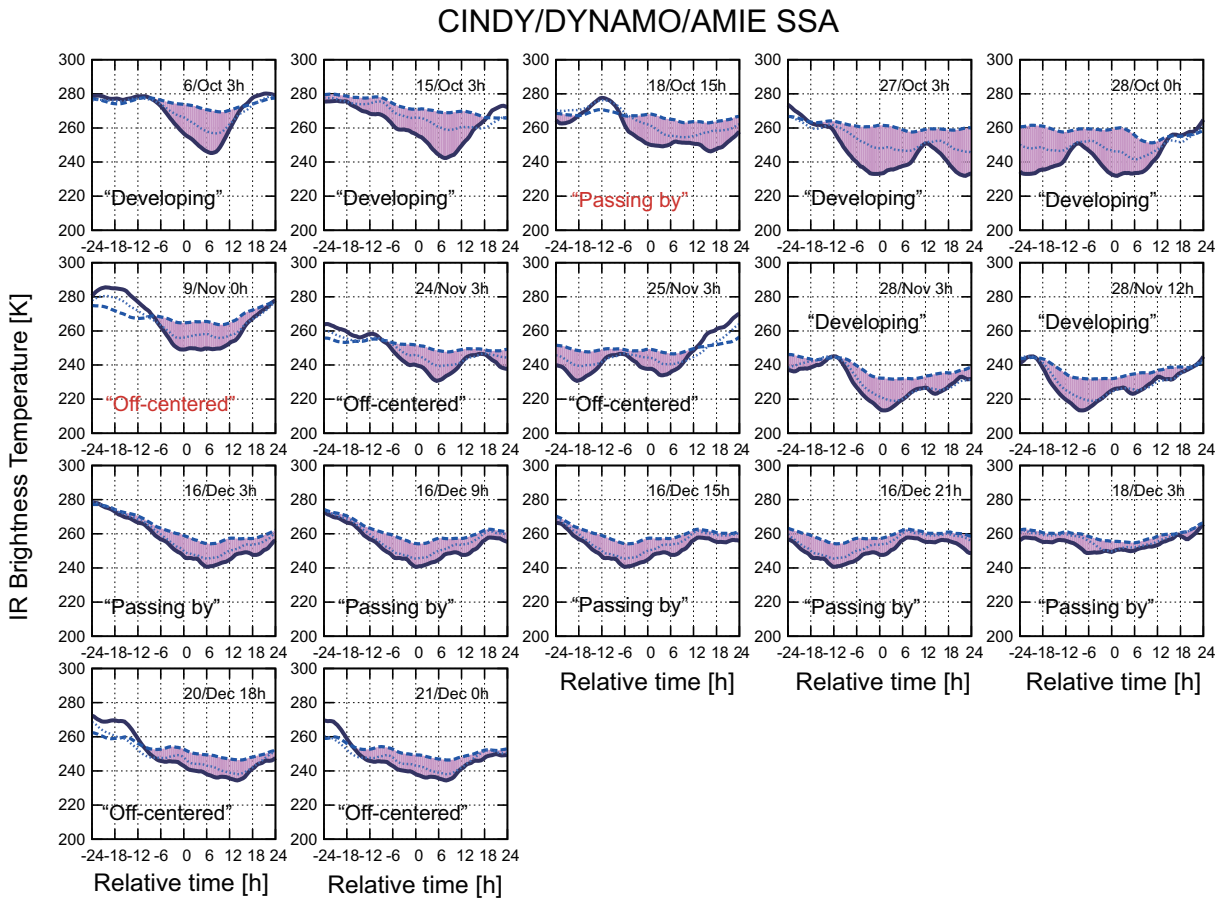
Fig. 8.   As Fig. 7 but for CINDY/DYNAMO SSA.

does not unambiguously fall in any one of the three composite classes. Observed disturbances more likely have hybrid properties that potentially ascribable to multiple classes at a time. Therefore, it is important to be aware that the identified classes claimed in Figs. 7 and 8 are not an unequivocal definition but a subjective reference for the primary (if not the sole) nature of individual disturbances.

4.2   Composite time series for different composite classes

All events observed in NSA and SSA (Figs. 4a, b) are grouped separately into the composite classes. Qualitative features of moisture convergence in all the classes (Fig. 10) are as expected from Fig. 4. However, the amplitude of the variability differs across the three classes; being most outstanding for developing disturbances, while barely visible in the passing-by class. This is also the case for MSE convergence plotted in Fig. 11, where the onset of

MSE divergence following the peak precipitation is sharpest in the developing class. It follows that the prominent characteristics in composite space, i.e., an enhancement of moisture convergence during convection and the subsequent outbreak of MSE divergence, may be principally attributed to the dynamic evolution of a convective system that completes its life cycle within the analysis domain. Off-centered and passing-by disturbances each occur as frequently as developing systems but are considered to be less responsible for the major features captured in Figs. 4 and 5. This result is supportive of the implicit conjecture underlying our analysis that major properties in composite space physically represent the convective development rather than mere advective effects. This conclusion arguably applies not only to the CINDY/DYNAMO measurements but also to the satellite observations as far as the underlying statistics are shared in common, which is a presumption corroborated to the extent suggested by the resem-
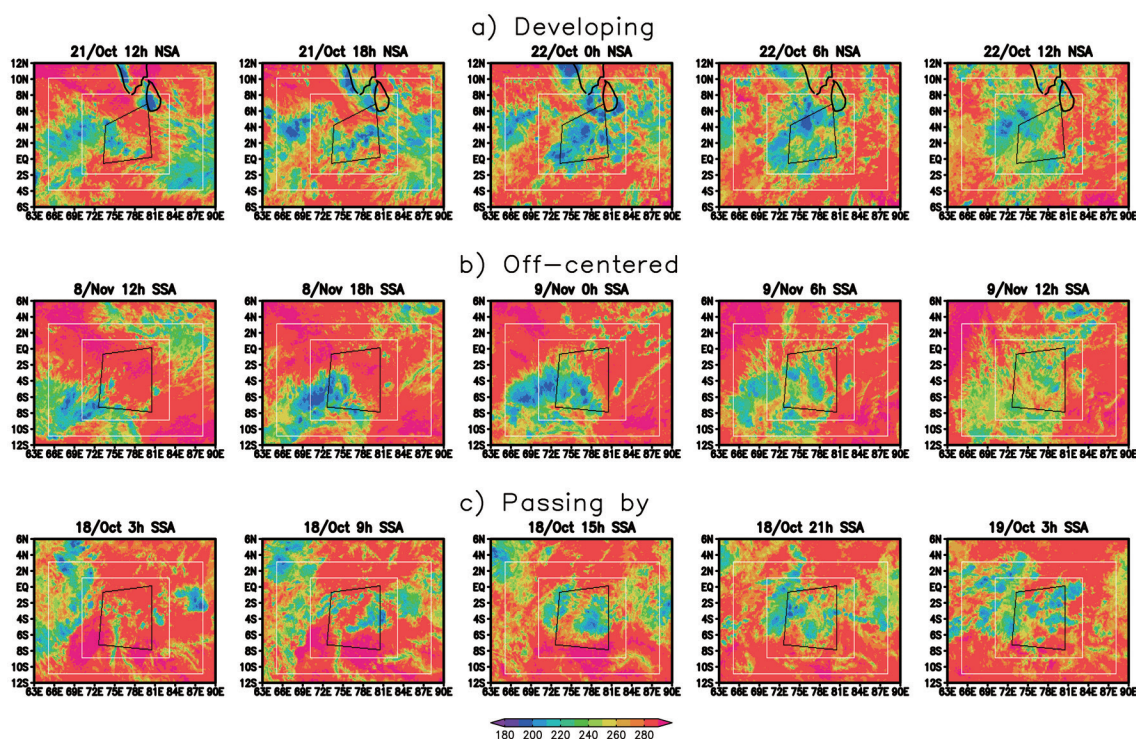
Fig. 9. Plan view of Meteosat infrared T_b for representative events selected for each composite class of (a) developing, (b) off-centered, and passing by. Five panels in each row are a sequence of 6-hourly snapshots centered around the time of peak precipitation (or the base point). A black quadrangle in each panel illustrates the sounding array and white boxes encompassing the array show the inner and outer fields.

blance between the satellite-based and sounding-array composites as confirmed earlier in Section 3.

5. Discussion

The composite time series from satellite observations was found to be in good agreement with the statistical properties of convective disturbances from the sounding-array measurements during CINDY/DYNAMO and TOGA COARE. Physical implications of the observed characteristics were discussed by Masunaga and L'Ecuyer (2014) as follows. The buildup of moisture convergence is brought by a low-level convergence associated with the first baroclinic mode, which develops following a modest, gradual increase of the positive second baroclinic (or congestus) mode. The positive second mode imports MSE against a preexisting weak MSE divergence and helps destabilize the atmosphere. Then, the second mode is switched in sign to a negative mode (or the stratiform mode), resulting in an abrupt onset of MSE divergence that leads to a restabilization of the atmosphere. The vertical profile of horizontal divergence calculated from a reanalysis dataset during the CINDY/DYNAMO by Zuluaga and Houze (2013) shows a composite temporal evolution closely parallel with the present result. A CINDY/DYNAMO budget analysis itself has revealed from convective heating estimates that transitions occur from shallow to deep convective and stratiform clouds (Johnson et al. 2015). A theoretical framework along the same line as above has been explored over the past decade (e.g., Peters and Bretherton 2006; Khouider and Majda 2006). However, there is a remaining concern that the systematic patterns observed in the ensemble mean are in general not visually recognizable in individual events. Potential origins for this include contaminating influences from other disturbances nearby. It is implicitly assumed so far that the large-scale environment is not affected by multiple convective systems at any given time. This assumption is obviously not guaranteed to be valid particularly for the events sampled from a synoptic-scale environment favorable for intensive convection such as the active MJO envelope.

(a) Developing

(b) Off-centered
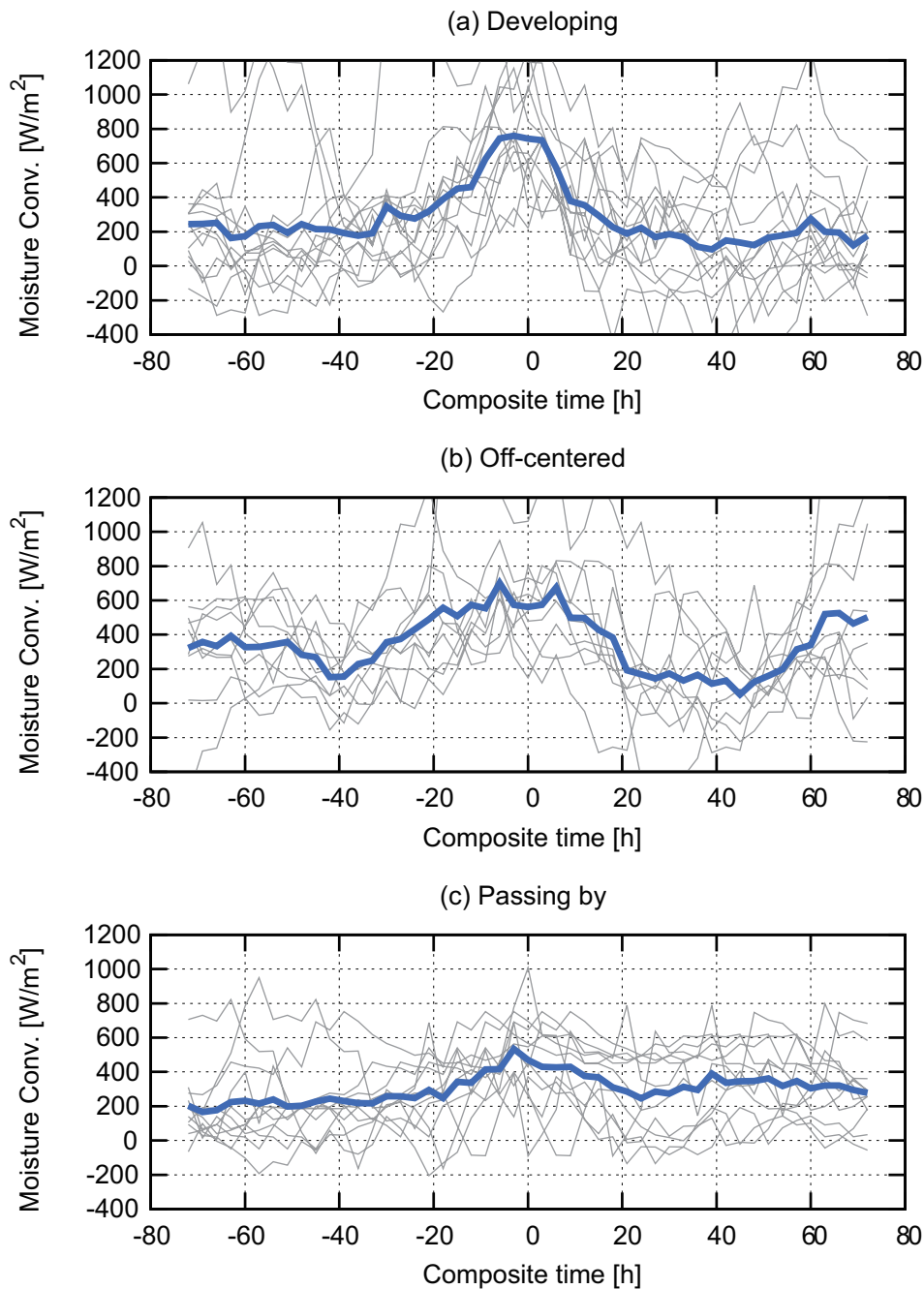
(c) Passing by

Fig. 10.   Vertically integrated moisture convergence [W m^{-2}] in composite space for the different composite classes: (a) Developing, (b) Off-centered, and (c) Passing by. Individual samples are drawn in gray and their ensemble mean in blue.

To minimize the contaminating effects from co-existing disturbances, convective events not under the apparent influence of the MJO during CINDY/DYNAMO are subjectively selected from Meteosat IR imagery to define "isolated" disturbances. Four isolated convective events (indicated by "I" in Fig. 1) are identified around October 16 (NSA), October 6 (SSA), October 15 (SSA), and November 9 (SSA).
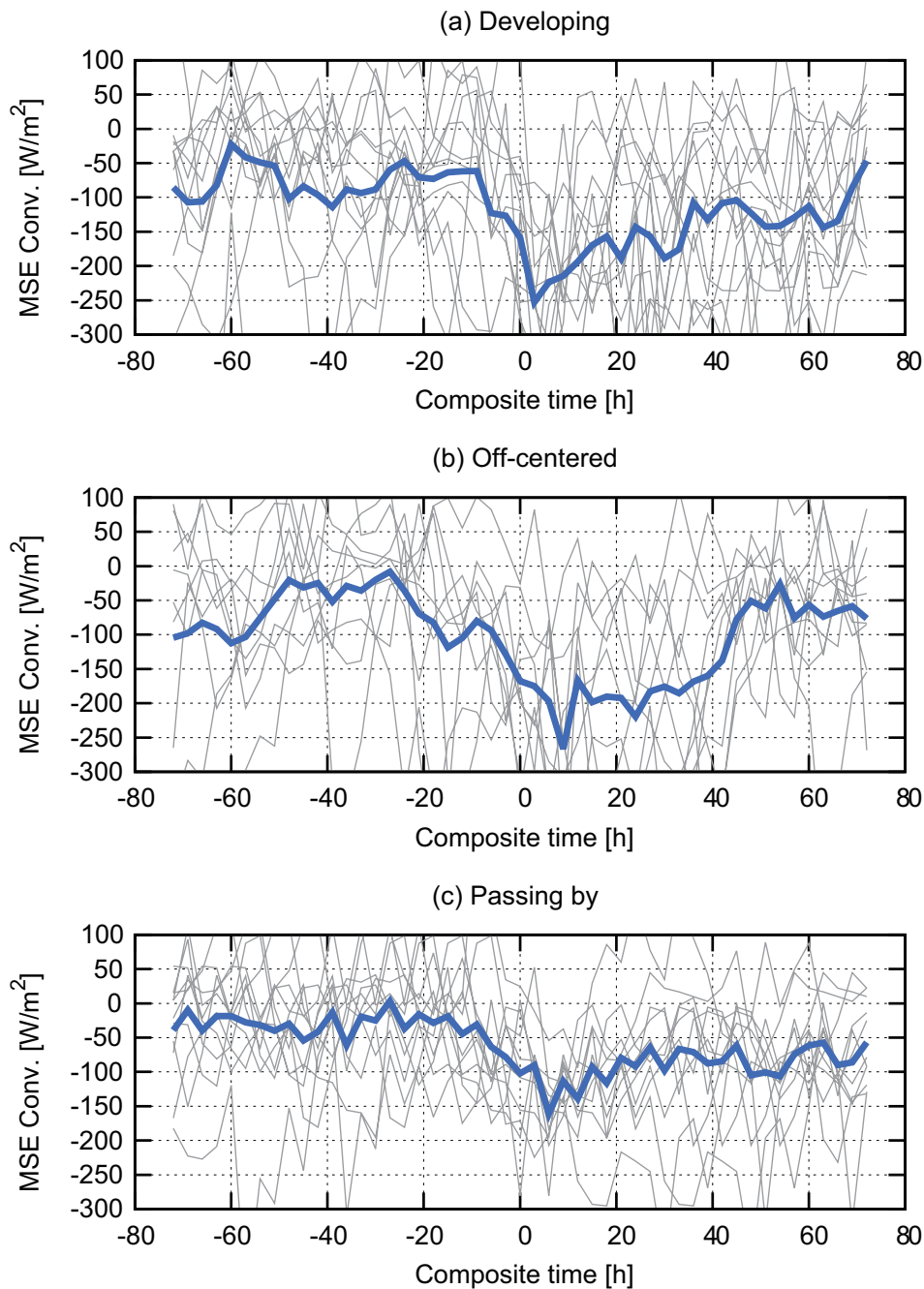
Fig. 11.   As Fig. 10 but for vertically integrated MSE convergence.

All the four events turn to follow a coherent track of moisture convergence even without averaging (Fig. 12a) but are heavily spread in MSE convergence particularly for positive hours (Fig. 12b). However, MSE convergence better converges into an evolutionary path reminiscent of the ensemble mean from

Fig. 5 when horizontal advection is excluded from the MSE convergence estimate (Fig. 12c). Vertically integrated convergence may be broken down into horizontal and vertical advections as shown in Eq. (7). The systematic evolution in terms of the vertical mode decomposition as described earlier is accounted
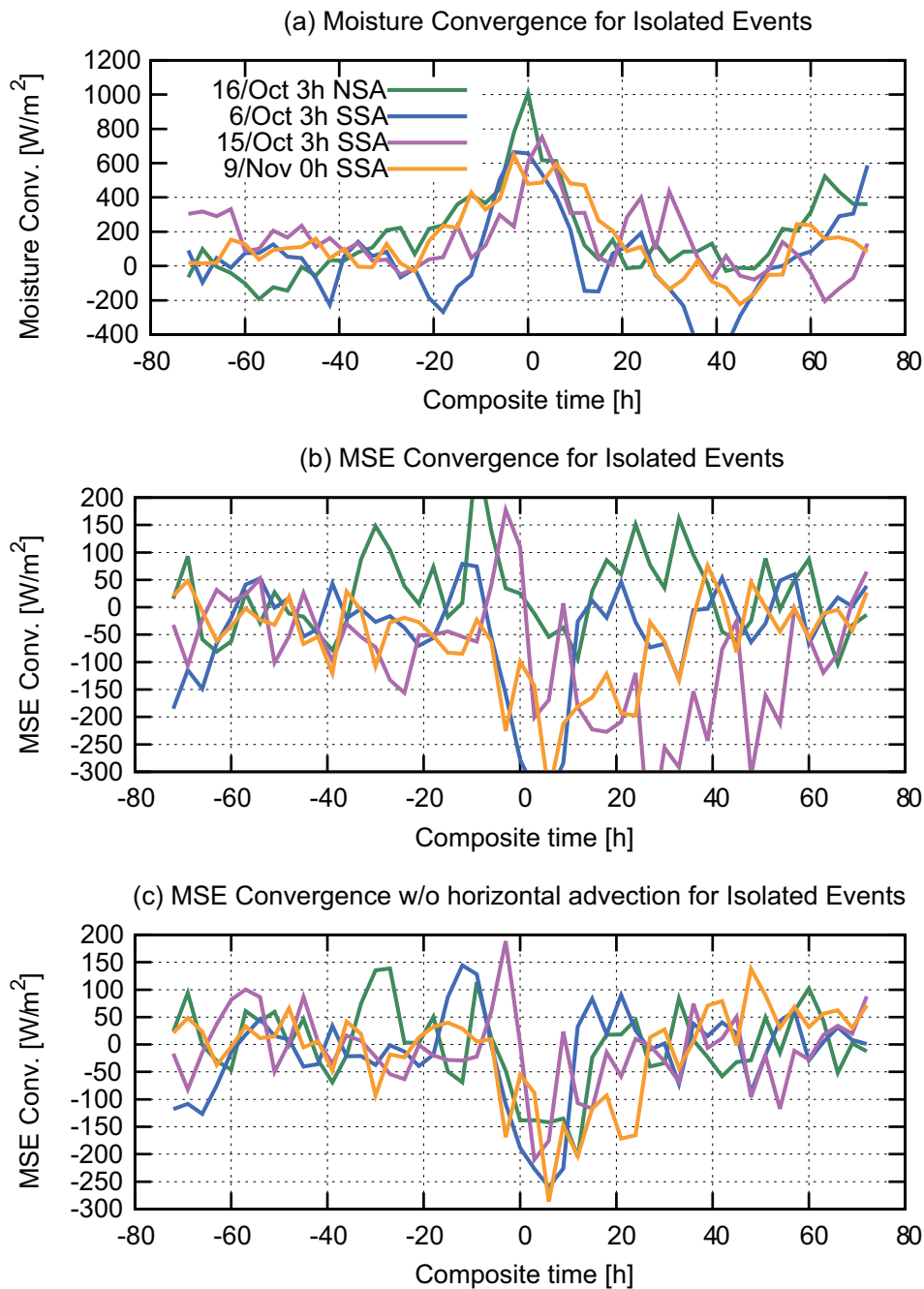
Fig. 12.   Composite time series for isolated convective events as indicated in the top panel. (a) Moisture convergence. (b) MSE convergence. (c) MSE convergence with the contribution of horizontal advection excluded.

for by vertical advection, largely intrinsic to the local dynamics. On the other hand, the horizontal advection of MSE depends on horizontal moisture gradient in the large-scale environment and could irregularly modulate the thermodynamic variability that other-

wise would be controlled by internal convective dynamics. While horizontal advection could play crucial roles in the driving mechanism of the MJO (e.g., Benedict and Randall 2007; Maloney 2009; Sobel et al. 2014), the relative magnitude of hori-

(a) Moisture Convergence Breakdown

(b) MSE Convergence Breakdown
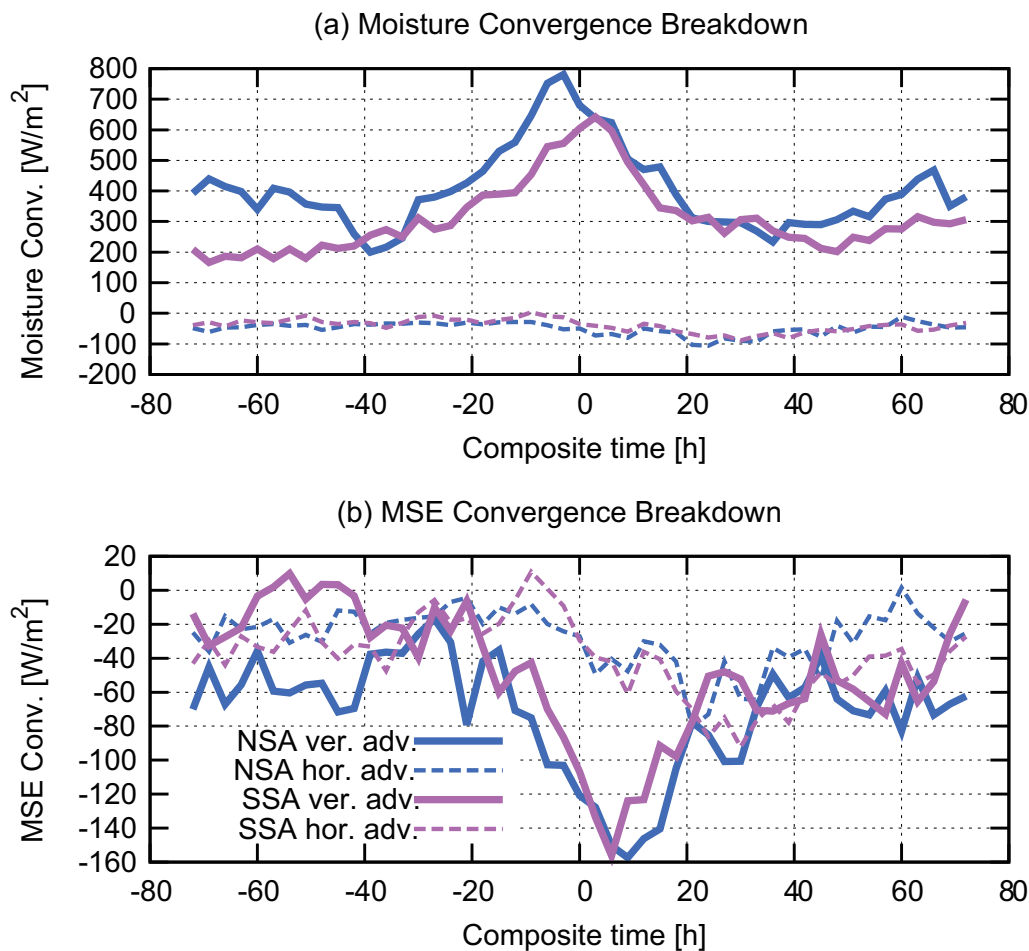
Fig. 13. CINDY/DYNAMO composites of the vertical integral of vertical advection (solid) and horizontal advection (dashed), which together account for vertically integrated convergence. (a) Moisture advections. (b) MSE advections.

zontal and vertical advections is dependent on the cycle of variability and the horizontal component is least important at daily time scales (Inoue and Back 2015). Figure 13 shows the breakdown of moisture/MSE convergence into horizontal and vertical advections calculated from the ensemble mean of all CINDY/DYNAMO events. Horizontal moisture advection stays weakly negative fluctuating between 0 and -100 W m^{-2}, nearly leaving vertical moisture advection to entirely account for moisture convergence (Fig. 13a). A rapid development of vertical moisture advection (or moisture convergence) is largely canceled by precipitation during the time of peak convection (Masunaga 2013; Chikira 2014). In the MSE budget, horizontal advection has a comparable magnitude to vertical advection during hours

away from $t\sim0$. On the other hand, vertical advection is solely responsible for the abrupt onset of MSE divergence after $t = 0$. These results are supportive of the present interpretation of the composite evolution from the perspective of large-scale vertical modes.

The satellite-based composite presented in this study is constructed with observations over all tropical oceans, although it would be desirable to limit satellite measurements to strictly over the sounding arrays for fair comparison with the field campaign data. However, such a local subset of the satellite composite would suffer from an intolerable level of sampling noise because the compositing technique requires a huge volume of observations to retain robust statistics. The present comparison relies on the underlying assumption that the regional climatology
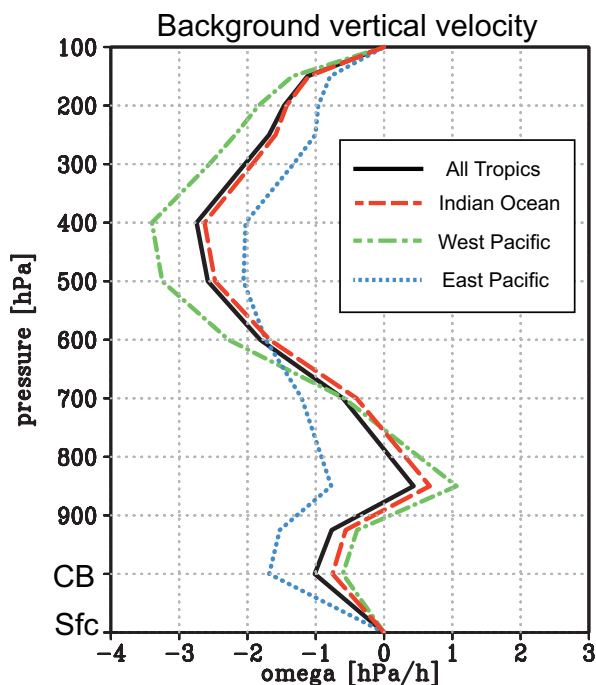
Fig. 14. Regional breakdown of background vertical velocity derived for the satellite-based composite: all tropical oceans (black solid), Indian Ocean (red dashed), west Pacific (green dot-dashed), and east Pacific (blue dotted).

specific to the CINDY/DYNAMO or TOGA COARE site is not critically different from the global tropical climatology. This is a speculation that has yet to be verified.

To this end, the regional climatology in large-scale dynamics is examined with background vertical velocity derived for the satellite-based composite. Figure 14 depicts the regional breakdown of background ω into the Indian Ocean (50°E–90°E), west Pacific (140°E–180°), and east Pacific (50°W–10°W), bound meridionally between 15°S and 15°N with islands excluded. All the profiles share common features including a weak top-heavy ascent and a shallow updraft, while the amplitude varies from one region to another. The Indian Ocean profile closely resembles the tropical mean over the entire thickness of the troposphere, implying that the present satellite-based composite is safely comparable with the CINDY/DYNAMO soundings. The west Pacific exhibits a stronger upper-tropospheric peak in the background ω profile than the tropical mean. This might be partially responsible for the difference between the satellite and TOGA COARE compos-

ites. In contrast, the east Pacific is characterized with a modest upper-tropospheric ascent and a robust shallow updraft compared to other regions as one might expect from the climatologically shallow circulation typical of this region (e.g., Zhang et al. 2004).

6.   Summary

A satellite-based method previously developed by the author for moisture and thermal budget analysis is assessed in comparison with sounding array measurements from CINDY/DYNAMO and TOGA COARE. The result shows that the composite time series of large-scale mean vertical motion from a suite of satellite observations closely resembles the sounding array estimates, whereas the satellite composite exhibits a shallow updraft in the background that is absent in the in-situ soundings. Moisture convergence and MSE convergence are qualitatively consistent between the satellite and sounding array composites, although a significant spread resides around the ensemble mean among individual convective events.

Convective disturbances are categorized into developing, off-centered, and passing-by classes using geostationary infrared measurements in attempt to separate irrelevant samples where convective development mainly takes place outside the array or disturbances pass over the array without experiencing systematic development. All the three cases are found qualitatively similar, except that developing events are greatest in the amplitude of variability while the variability becomes less coherent for off-centered and passing-by disturbances. It follows that the fundamental large-scale thermodynamics associated with convective development is reasonably captured in the satellite composite to the extent not to be heavily distorted by stochastic influences from the environment. In fact, moisture convergence plotted for individual events converges into a coherent evolution resembling the ensemble mean when the convective events immune to apparent synoptic-scale influences are isolated. This is also the case for MSE convergence once the contribution of horizontal advection is excluded. Vertical advection is largely responsible for the notable evolutionary properties characterizing moisture and MSE convergences, although horizontal advection has a comparable contribution to MSE convergence during spells without vigorous convection.

References

Aumann, H. H., M. T. Chahine, C. Gautier, M. Goldberg, E. Kalnay, L. McMillin, H. Revercomb, P. W. Rosenkranz, W. L. Smith, D. Staelin, L. Strow, and J. Susskind, 2003: AIRS/AMSU/HSB on the Aqua mission: Design, science objectives, data products, and processing systems. *IEEE Trans. Geosci. Remote Sens.*, **41**, 253–264.

Benedict, J. J., and D. A. Randall, 2007: Observed characteristics of the MJO relative to maximum rainfall. *J. Atmos. Sci.*, **64**, 2332–2354.

Chikira, M., 2014: Eastward-propagating intraseasonal oscillation represented by Chikira-Sugiyama cumulus parameterization. Part II: Understanding moisture variation under weak temperature gradient balance. *J. Atmos. Sci.*, **71**, 615–639.

Ciesielski, P. E., R. H. Johnson, P. T. Haertel, and J. Wang, 2003: Corrected TOGA COARE sounding humidity data: Impact on diagnosed properties of convection and climate over the warm pool. *J. Climate*, **16**, 2370–2384.

Huffman, G. J., R. F. Adler, D. T. Bolvin, G. Gu, E. J. Nelkin, K. P. Bowman, Y. Hong, E. F. Stocker, and D. B. Wolff, 2007: The TRMM multi-satellite precipitation analysis (TMPA): Quasi-global, multiyear, combined-sensor precipitation estimates at fine scales. *J. Hydrometeor.*, **8**, 38–55.

Inoue, K., and L. E. Back, 2015: Column-integrated moist static energy budget analysis on various time scales during TOGA COARE. *J. Atmos. Sci.*, **72**, 1856–1871.

Johnson, R. H., and P. E. Ciesielski, 2013: Structure and properties of Madden-Julian oscillations deduced from DYNAMO sounding arrays. *J. Atmos. Sci.*, **70**, 3157–3179.

Johnson, R. H., P. E. Ciesielski, J. H. Ruppert, Jr., and M. Katsumata, 2015: Sounding-based thermodynamic budgets for DYNAMO. *J. Atmos. Sci.*, **72**, 598–622.

Khouider, B., and A. J. Majda, 2006: A simple multicloud parameterization for convectively coupled tropical waves. Part I: Linear analysis. *J. Atmos. Sci.*, **63**, 1308–1323.

Maloney, E. D., 2009: The moist static energy budget of a composite tropical intraseasonal oscillation in a climate model. *J. Climate*, **22**, 711–729.

Masunaga, H., 2012a: A satellite study of the atmospheric forcing and response to moist convection over tropical and subtropical oceans. *J. Atmos. Sci.*, **69**, 150–167.

Masunaga, H., 2012b: Short-term versus climatological relationship between precipitation and tropospheric humidity. *J. Climate*, **25**, 7983–7990.

Masunaga, H., 2013: A satellite study of tropical moist convection and environmental variability: A moisture and thermal budget analysis. *J. Atmos. Sci.*, **70**, 2443–2466.

Masunaga, H., 2014: Free-tropospheric moisture convergence and tropical convective regimes. *Geophys. Res. Lett.*, **41**, 8611–8618.

Masunaga, H., and T. S. L'Ecuyer, 2014: A mechanism of tropical convection inferred from observed variability in the moist static energy budget. *J. Atmos. Sci.*, **71**, 3747–3766.

Neelin, J. D., and I. M. Held, 1987: Modeling tropical convergence based on the moist static energy budget. *Mon. Wea. Rev.*, **115**, 3–12.

Peters, M. E., and C. S. Bretherton, 2006: Structure of tropical variability from a vertical mode perspective. *Theor. Comput. Fluid Dyn.*, **20**, 501–524.

Powell, S. W., and R. A. Houze, Jr., 2013: The cloud population and onset of the Madden-Julian oscillation over the Indian Ocean during DYNAMO-AMIE. *J. Geophys. Res. Atmos.*, **118**, 11979–11995.

Raymond, D. J., S. L. Sessions, A. H. Sobel, and Ž. Fuchs, 2009: The mechanics of gross moist stability. *J. Adv. Model. Earth Syst.*, **1**, 9, doi:10.3894/JAMES.2009.1.9.

Reed, R. J., and E. E. Recker, 1971: Structure and properties of synoptic-scale wave disturbances in the equatorial western Pacfic. *J. Atmos. Sci.*, **28**, 1117–1133.

Sobel, A. H., S. Wang, and D. Kim, 2014: Moist static

energy budget of the MJO during DYNAMO. *J. Atmos. Sci.*, **71**, 4276–4291.

Trenberth, K. E., D. P. Stepaniak, and J. M. Caron, 2000: The global monsoon as seen through the divergent atmospheric circulation. *J. Climate*, **13**, 3969–3993.

Webster, P. J., and R. Lukas, 1992: TOGA COARE: The coupled ocean-atmosphere response experiment. *Bull. Amer. Meteor. Soc.*, **73**, 1377–1416.

Yanai, M., 1961: A detailed analysis of typhoon formation. *J. Meteor. Soc. Japan*, **39**, 187–214.

Yanai, M., S. Esbensen, and J.-H. Chu, 1973: Determination of bulk properties of tropical cloud clusters from large-scale heat and moisture budgets. *J. Atmos. Sci.*, **30**, 611–627.

Yoneyama, K., C. Zhang, and C. N. Long, 2013: Tracking pulses of the Madden-Julian oscillation. *Bull. Amer. Meteor. Soc.*, **94**, 1871–1891.

Zhang, C., M. McGauley, and N. A. Bond, 2004: Shallow meridional circulation in the tropical eastern Pacific. *J. Climate*, **17**, 133–139.

Zhang, C., D. S. Nolan, C. D. Thorncroft, and H. Nguyen, 2008: Shallow meridional circulations in the tropical atmosphere. *J. Climate*, **21**, 3453–3470.

Zuluaga, M. D., and R. A. Houze, Jr., 2013: Evolution of the population of precipitating convective systems over the equatorial Indian Ocean in active phases of the Madden-Julian oscillation. *J. Atmos. Sci.*, **70**, 2713–2725.